Acta Crystallographica Section A
Foundations of Crystallography
ISSN 0108-7673

Received 2 November 2010
Accepted 9 December 2010

Interference fringes in multiple Bragg–Laue mode

Tomoe Fukamachi,[a]* Kenji Hirano,[a] Riichirou Negishi,[a] Yoshinobu Kanematsu,[a] Sukswat Jongsukswat,[a] Keiichi Hirano[b] and Takaaki Kawamura[c]

[a]Saitama Institute of Technology, 1690 Fusaiji, Fukaya, Saitama 369-0293, Japan, [b]Institute of Material Structure Science, KEK-PF, High Energy Accelerator Research Organization, Oho, Tsukuba, Ibaraki 305-0801, Japan, and [c]Department of Mathematics and Physics, University of Yamanashi, Kofu, Yamanashi 400-8510, Japan. Correspondence e-mail: tomoe@sit.ac.jp

Interference fringes in multiple Bragg–Laue mode have been measured from the lateral surface of an Si plane-parallel crystal by changing the distance L between the incident point of X-rays and the crystal edge for two sample crystals with different thicknesses H. The period of the interference fringes becomes large when the distance L becomes large or the thickness H becomes small. When the ratio L/H is larger than 15, a shorter period of oscillation appears in addition to the interference fringes. These variations are explained by considering the beams in multiple Bragg–Laue modes based on the dynamical theory of diffraction. When L/H is less than 15, the measured fringes are well reproduced by taking account of interference between beams in the Bragg–Laue and the Bragg–Bragg–Laue modes. The short period of the oscillations observed for $L/H > 15$ is reproduced by adding the intensities of the beams in higher-order Bragg–Laue mode. The interference fringes calculated by taking the visibility into account show good agreement with the measured ones.

1. Introduction

X-ray interference fringes in diffraction from the lateral surface of a Ge plane-parallel crystal were reported by Fukamachi *et al.* (2004, 2005). The diffraction condition of the incident beam was the Bragg mode and that of the diffraction beams was the Laue mode. The cause of the fringes was attributed to interference between the beam in the Bragg–Laue (BL) mode and that in the Bragg–Bragg–Laue (BBL) mode as the incident X-ray was to be regarded as a spherical wave (Hirano *et al.*, 2008, 2009*a*,*b*). A schematic drawing of the beam arrangements in BL and BBL modes is shown in Fig. 1(*a*). It was pointed out by Yoshizawa *et al.* (2008) that the refracted beam in the crystal propagates in the direction of the corresponding Poynting vector. In Fig. 1(*a*), the refracted beams corresponding to the Poynting vectors in BL and BBL modes are denoted as $S_{\rm BL}$ and $S_{\rm BBL}$, respectively.

In these studies, the X-ray energy was set near the K absorption edge of Ge and the linear absorption coefficient was minimized as a result of anomalous transmission due to the Borrmann effect. The period of the fringes was inversely proportional to the crystal thickness and the crystal structure factor. The interference fringes were distorted by lattice distortion in the crystal and the period of the fringes was partly distorted by roughness of the crystal surfaces. The interference fringes can be applied not only to determine the crystal structure factor but also to investigate dislocations in a crystal. When the distance L between the incident point and the edge of the crystal is much longer than the crystal thickness H, as shown in Fig. 1(*b*), the refracted beam in the BB^2L mode reaches the lateral surface. If L is approximately four times longer than $H/\tan\theta_{\rm B}$, where $\theta_{\rm B}$ is the Bragg angle, the

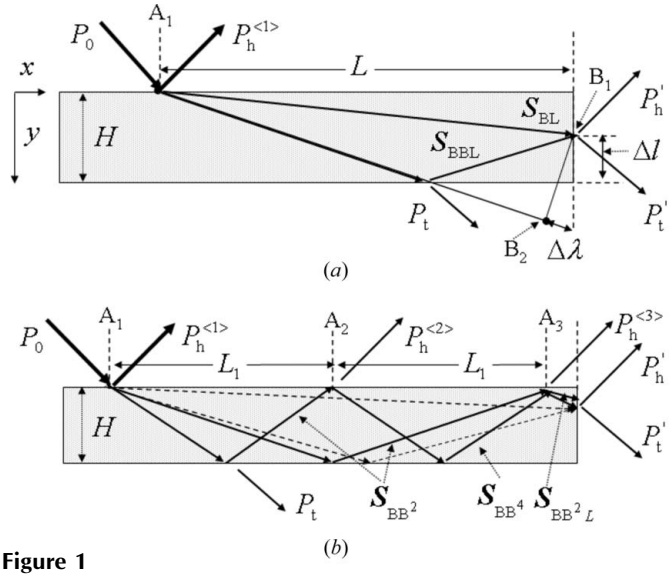

Figure 1
Schematic illustration of the beam geometry of MBL modes. L is the distance between the incident point of X-rays and the edge of the crystal, and H is the crystal thickness. The beam geometries of (*a*) BL and BBL modes, and (*b*) BB^mL modes from $m = 0$ to $m = 4$ are shown. **S** represents the Poynting vector and its suffix BB^mL modes. $P'_{\rm h}$ and $P'_{\rm t}$ represent the intensities of diffraction from the lateral surface in the diffracted- and transmitted-beam directions, respectively. If Δl is the region where the MBL interference fringes are observed, $\Delta\lambda$ is the coherent length, because $A_1B_1 = A_1B_2$.

refracted beams in the multiple Bragg–Laue (BB^{m}L or MBL) mode reach the lateral surface with integer m being larger than 2. When the refracted beam comes out from the surface at A_2 after reflection at the bottom surface, the diffracted beam $P_h^{\langle 2\rangle}$ is observed. When the refracted beams in the BB^2 and BB^4 modes come out of the surface at A_3, the interference between these reflected beams should be observed in the reflected beam $P_h^{\langle 3\rangle}$. In this case, the distance between A_1 and A_3 is twice that between A_1 and A_2.

In this paper, the interference fringes in diffraction from the lateral surface of an Si plane-parallel crystal are reported. The X-ray energy is approximately 11 100 eV, which is much higher than the K absorption edge of Si (1840 eV), and the effect of the anomalous scattering factor is quite small. It is expected that the interference fringes between beams in the BL mode and those in MBL modes should be observed without a large intensity decrease, and that the number of the interference fringes should be increased by increasing the crystal thickness. The increase in the number of fringes is important for applications such as X-ray interferometry.

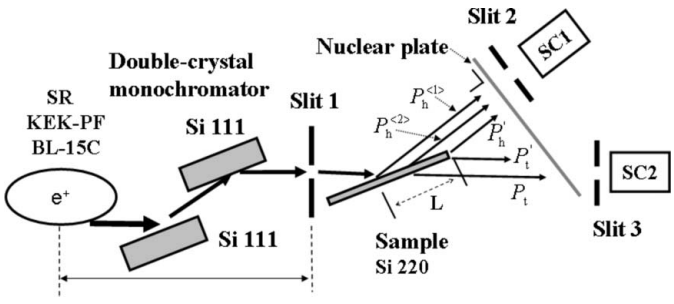

Figure 2
Schematic diagram of the measuring system. SR, synchrotron radiation X-ray source; SC, scintillation counter.

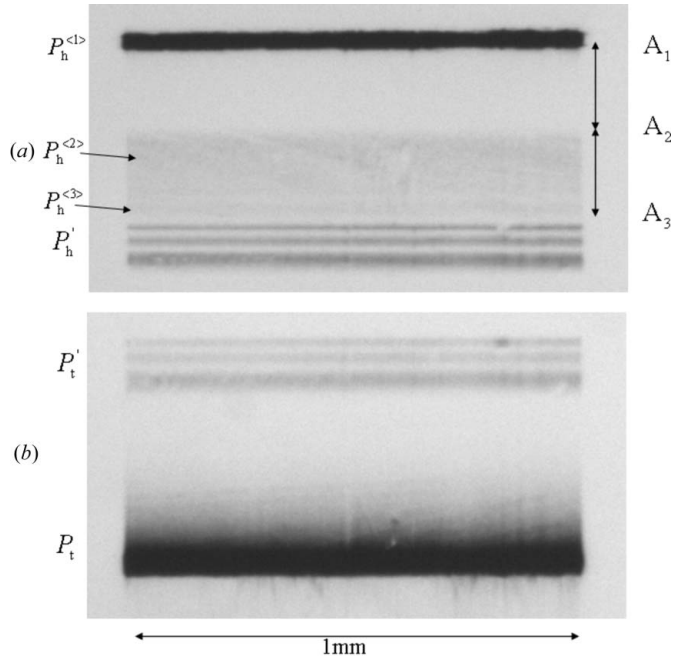

Figure 3
Photographs of the diffraction intensities P_h and P_h' (a), and P_t and P_t' (b). The crystal thickness of Si is 110 µm and the distance L = 1440 µm. In (a), $P_h^{(1)}$, $P_h^{(2)}$ and $P_h^{(3)}$ are the diffracted beams in the Bragg, BB^2 and BB^4 modes, respectively.

2. Experimental

Two plane-parallel Si crystals used in the experiment were cut from a wafer 0.3 mm thick and 100 mm in diameter. One sample was 40 mm long, 10 mm wide and 0.11 mm thick, and the other sample was 50 mm long, 10 mm wide and 0.18 mm thick, after mechanical–chemical polishing.

The experiments were carried out using X-rays from synchrotron radiation at BL-15C, Photon Factory, KEK, Tsukuba, Japan. The X-rays were σ-polarized and monochromated using an Si 111 double-crystal monochromator. The X-ray energy was 11 100 $\pm$ 0.5 eV. The measuring system is shown schematically in Fig. 2. The vertical and horizontal widths of the beam after slit 1 were 30 and 1000 µm, respectively. The transmitted-beam P_t and the diffracted-beam $P_h^{\langle n\rangle}$ intensities as well as the emitted-beam intensities from the lateral surface in the transmitted (P_t')- and diffracted (P_h')-beam directions were recorded on the nuclear plates and measured by scintillation counters.

3. Results

Photographs of the diffracted intensities recorded in the diffracted- and transmitted-beam directions are shown in Fig. 3. The sample's thickness is 110 µm and the distance L is 1440 µm. $P_h^{(1)}$ is the diffracted intensity in the Bragg mode, $P_h^{(2)}$ is that in BB^2 mode and $P_h^{(3)}$ is that in BB^4 mode coupled with that in BB^2 mode as shown in Fig. 1(b). P_h' is the emitted

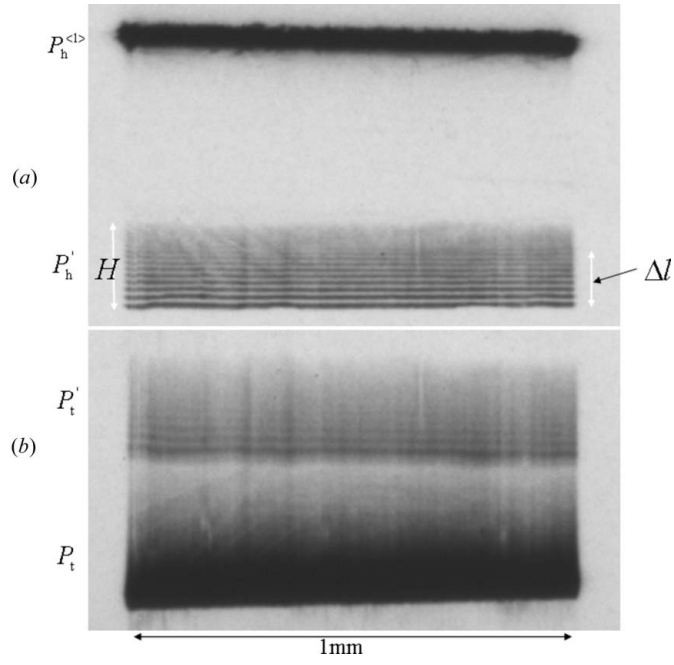

Figure 4
Photographs of the diffraction intensities $P_h^{(1)}$ and P_h' (a), and P_t and P_t' (b). The crystal thickness of Si is 180 µm and the distance L = 1390 µm.

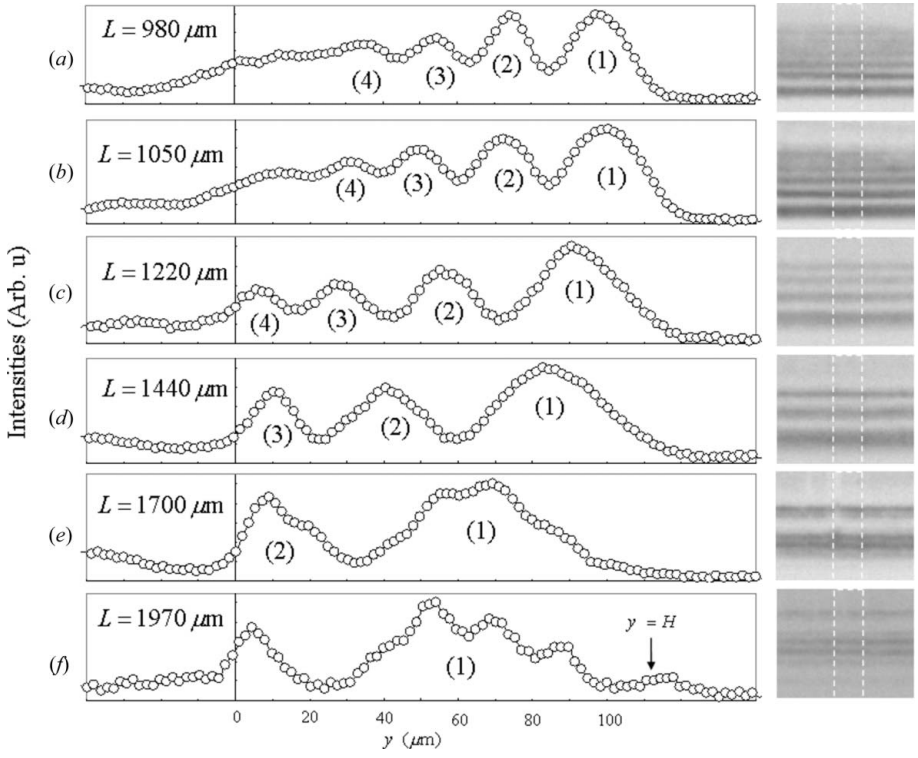

Figure 5
Photographs of P'_h (right) and the corresponding intensity profiles of P'_h (left) in MBL modes. The sample thickness is 110 μm. The distances L are (*a*) 980, (*b*) 1050, (*c*) 1220, (*d*) 1440, (*e*) 1700 and (*f*) 1970 μm.

In Fig. 5 are shown photographs of P'_h (right) and their intensity profiles (left) along the vertical direction y read from the photographs. The distance L changes as (*a*) 980, (*b*) 1050, (*c*) 1220, (*d*) 1440, (*e*) 1700 and (*f*) 1970 μm. The thickness of the crystal is 110 μm. When L increases from 980 to 1440 μm, the number of interference fringes decreases from four to three. In Figs. 5(*e*) and 5(*f*), a shorter period of oscillations appears in addition to the interference fringes. When the thickness of the crystal is 180 μm and L is 1390 μm, the intensity profile of P'_h changes as shown in Fig. 6. As the distance L of 1390 μm in Fig. 6 is similar to that of 1440 μm in Fig. 5(*d*), the different intensity profiles between these two should be caused by the difference in crystal thickness. The number of interference fringes in Fig. 6 is ten, which is approximately three times larger than in Fig. 5(*d*).

intensity from the lateral surface in the diffracted-beam direction. P_t is the transmitted intensity and P'_t the emitted-beam intensity from the lateral surface in the transmitted-beam direction. Three periods of interference fringes are observed both in P'_h and P'_t. Similar diffracted intensities from the 180 μm-thick sample crystal are shown in Fig. 4 by setting L = 1390 μm. Ten and five periods of interference fringes are observed in P'_h and P'_t, respectively. No intensity maximum such as $P_h^{(2)}$ and $P_h^{(3)}$ is observed between $P_h^{(1)}$ and P'_h.

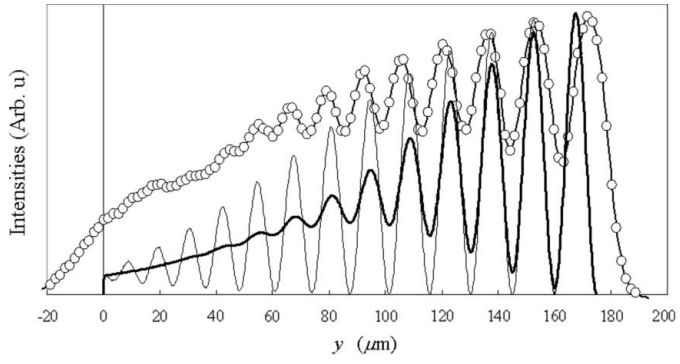

Figure 6
Measured intensity profiles of MBL fringes (circles). The sample thickness is 180 μm and L = 1390 μm. The thick solid and the thin solid lines show the calculated intensities as a function of y for $\Delta\lambda$= 26 μm and $\Delta\lambda = \infty$, respectively. The sample thickness is assumed to be 175 μm.

4. Theoretical basis

Under the present experimental conditions, the refracted beam is regarded as a spherical wave. A part of the spherical wave S_{BL} in BL mode and another part S_{BBL} in BBL mode can interfere with each other and come out from the lateral surface as shown in Fig. 1(*a*). These two beams cause the interference fringes observed in the diffraction from the lateral surface. The electric field at the lateral surface in the diffracted-beam direction denoted as E'_h can be given by

$$E'_h = E_{BL}\exp(i2\pi\theta_1) + E_{BBL}\exp(i2\pi\theta_2). \quad (1)$$

The first term on the right-hand side expresses the electric field in BL mode and the second term that in BBL mode. The electric fields are given by $E_{BL} = \Omega_{BL}A_1\kappa_1 D_h^{1(1)}$ and $E_{BBL} = \Omega_{BBL}A_2\kappa_2 D_h^{1(2)}$ with Ω_{BL} and Ω_{BBL} being the correction factors due to the beam width (Authier, 2001; Hirano *et al.*, 2008, 2009*a*,*b*). A_1 and A_2 are the correction factors due to absorption, and κ_1 and κ_2 the correction factors due to the size of the dispersion surface. The electric displacement $D_h^{1(j)}$ is related to the incident electric field E_0 as $D_h^{1(j)} = r^{(j)}E_0$. The superscript '1' represents the first-order reflection. The superscript (j) represents the branch number. The branch j = 1 corresponds to the beam propagating in the transmitted direction such as that in BL mode and the branch j = 2 corresponds to the beam propagating in the diffracted-beam direction such as that in BBL mode. The reflection coefficient is given by $r^{(j)} = D_h^{(j)}/D_0^{(j)}$ with $D_0^{(j)}$ and $D_h^{(j)}$ being the electric displacements in the transmitted- and diffracted-beam directions, respectively. The diffracted intensity $P'_h = |E'_h|^2$ is given by

$$P'_{\rm h} = |E_{\rm BL} + E_{\rm BBL}\exp(i2\pi\Delta\theta)|^2. \quad (2)$$

The phase factor is expressed as

$$\Delta\theta = \theta_2 - \theta_1 = \Delta\theta_x + \Delta\theta_y \quad (3)$$

with

$$\Delta\theta_x = k_{x2}x_2 - k_{x1}x_1 \quad \text{and} \quad \Delta\theta_y = k_{y2}y_2 - k_{y1}y_1. \quad (4)$$

Here k_x and k_y are X and Y components of the wavevector of the refracted wave, $k_{x1}x_1$ and $k_{y1}y_1$ are the corresponding phase factors in BL mode, and $k_{x2}x_2$ and $k_{y2}y_2$ those in BBL mode. Since the distances x_1 and x_2 are both set to be L and the relation

$$k_{x2} - k_{x1} = k_{0x} + X_2 - (k_{0x} + X_1) = X_2 - X_1 \quad (5)$$

holds according to the dispersion surface in Fig. 7, the phase $\Delta\theta_x$ can be obtained as

$$\Delta\theta_x = (X_2 - X_1)L. \quad (6)$$

As $k_{y1} = |\mathbf{h}|/2 + Y_1$ and $k_{y2} = |\mathbf{h}|/2 + Y_2$, the phase $\Delta\theta_y$ can be given by

$$\Delta\theta_y = (1/2d)(y_2 - y_1) + (Y_2y_2 - Y_1y_1). \quad (7)$$

Here, $\mathbf{h}$ is a reciprocal-lattice vector and is related to the lattice spacing (d) as $d = 1/|\mathbf{h}|$. The first term on the right-hand side of equation (7) shows an oscillation with the period of lattice spacing, which does not contribute to the MBL oscillations with a period of μm order. Then the phase factor of the MBL oscillation can be given by

$$\Delta\theta = (X_2 - X_1)L + Y_2y_2 - Y_1y_1. \quad (8)$$

Once the exit position on the lateral surface is given, that is y is given as shown in Fig. 8 and the refracted-beam direction $S_{\rm BL}^{(1)}$ is given, the corresponding deviation parameter W (Hirano *et al.*, 2009*a*,*b*) and the tie point (X, Y) on the dispersion surface are fixed as can be seen in Fig. 7. The y coordinate on the lateral surface is given by $y = y_1$ and $y_2 = 2H - y_1$, as shown in Fig. 8. In the photographs of Fig. 3, the diffraction in the BB^2 mode is also observed as denoted by $P_{\rm h}^{(2)}$. The diffracted intensity is given by

$$P'_{\rm h} = |E_{\rm BL} + E_{\rm BBL}\exp(i2\pi\Delta\theta_{21}) + E_{\rm BB2L}\exp(i2\pi\Delta\theta_{31})|^2. \quad (9)$$

The third term represents the contribution from the electric field $E_{\rm BB^2L}$ in BB^2L mode. $\Delta\theta_{21} = \theta_2 - \theta_1$ and $\Delta\theta_{31} = \theta_3 - \theta_1$.

5. Discussion

5.1. Visibility

In Fig. 6, the circles show the intensities of the measured interference fringes from a thick crystal (H = 180 μm), as in Fig. 4. The thin solid line shows the calculated interference fringes between the diffractions in BL and BBL modes by assuming infinite coherent length. The value of the thickness used in the calculation is chosen so as to fit the measured oscillation, which is 175 μm and slightly smaller than the measured value (H = 180 μm). As the sample slice is not a perfectly plane-parallel crystal and roughness of the order of several μm exists on the surface with mechanical–chemical polishing, the measured thickness should be the upper limit.

The agreement in period of the interference fringes between the measurement and calculation is quite good, although the calculated amplitudes of the fringes at $y = 0$ are much larger than the measured amplitudes. In the interference fringes, the path lengths of the beams in BL mode and those in BBL mode are different, in addition to the difference in the wavevectors in these two modes. The coherent length $\Delta\lambda$ can be estimated by measuring the region Δl at which the interference fringes are observed, as shown in Fig. 1(*a*). If the coherent length is given, the interference component α of the fringes can be obtained assuming that α is given by $\exp[-(H - y)^2/\Delta l^2]$. The thick, solid line in Fig. 6 shows the

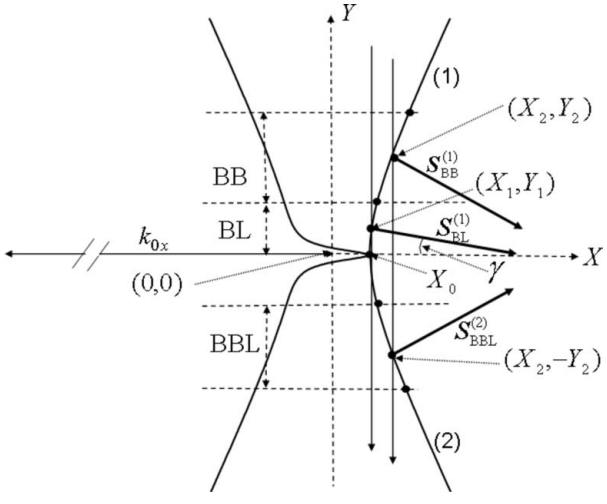

Figure 7
Dispersion surface. The Poynting vectors $\mathbf{S}_{\rm BL}^{(1)}$, $\mathbf{S}_{\rm BB}^{(1)}$ and $\mathbf{S}_{\rm BBL}^{(2)}$ start at the tie points (X_1, Y_1), (X_2, Y_2) and (X_2, $-Y_2$), respectively. $X_1 = W_1X_0$ and $X_2 = W_2X_0$.

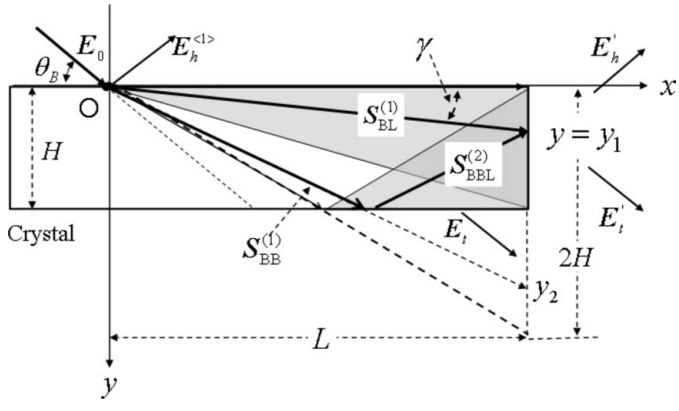

Figure 8
Paths of the refracted beams of the Poynting vectors $\mathbf{S}_{\rm BL}^{(1)}$ and $\mathbf{S}_{\rm BBL}^{(2)}$ in BL and BBL modes. E_0 is the electric field of the incident X-ray. $E_{\rm h}^{(1)}$ and $E'_{\rm h}$ are the electric field of the diffracted beam and that of the beam from the lateral surface in the direction of the diffracted beam. $E_{\rm t}^{(1)}$ and $E'_{\rm t}$ are the electric field of the transmitted beam and that of the beam from the lateral surface in the direction of the transmitted beam.

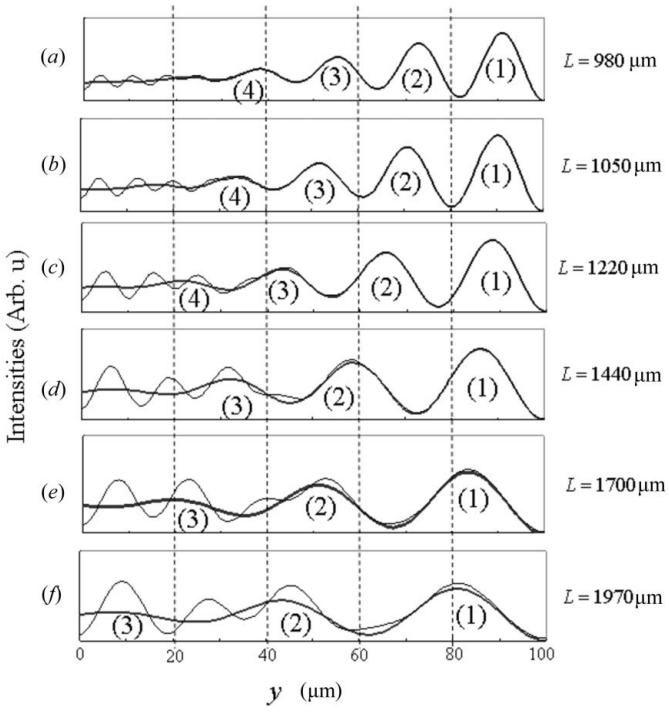

Figure 9
Calculated intensity profiles of P'_h by taking account of the beams in BL and BBL modes (thick solid line) and the beams in BL, BBL and BB^2L modes (thin solid line). The distance L is (*a*) 980, (*b*) 1050, (*c*) 1220, (*d*) 1440, (*e*) 1700 and (*f*) 1970 μm. The crystal thickness is taken to be 100 μm.

calculated interference fringes after correction by α. The calculated amplitudes of the fringes after this correction reproduce quite well the disappearance of the oscillation in the region $y < 40$ μm.

In Fig. 9, the thick solid lines show the calculated intensity profiles of the interference fringes P'_h between the diffractions in BL and BBL modes. In this case, the estimated coherent length $\Delta\lambda$ is 16 μm. The distance L is assumed to be (*a*) 980, (*b*) 1050, (*c*) 1220, (*d*) 1440, (*e*) 1700 and (*f*) 1970 μm corresponding to the values in Fig. 5. The agreement between the measured profiles in Figs. 5(*a*)–(*c*) with the calculated profiles in Figs. 9(*a*)–(*c*) is quite good when $H/L < 15$. The small additional oscillation of shorter period shown in Figs. 5(*e*) and 5(*f*) is not seen in the calculated curves of Figs. 9(*e*) and 9(*f*) when the condition $H/L > 15$ is satisfied. In Fig. 9, the thin lines show the calculated interference fringes by adding the diffraction in BB^2L mode as given in equation (9). The additional oscillations of shorter period are well reproduced. The calculated period of the oscillations in Figs. 9(*e*) and 9(*f*) is slightly larger than the measured period in Figs. 5(*e*) and 5(*f*).

Each peak (1) in Fig. 9 appears at a larger value of y than the corresponding peak position in Fig. 5. For larger L, the difference in peak position is larger. This displacement of the peak positions should be attributed to crystal bending, as pointed out by Saka & Kato (1986), which will be discussed in §5.4.

5.2. Confined beam effect

In Fig. 5(*f*), a small peak appears at $y = H$ as indicated by an arrow. This peak does not move and is not caused by the interference between diffractions in MBL modes but is caused by the confined beam effect (Fukamachi *et al.*, 2006; Hirano *et al.*, 2008, 2009*a*,*b*). The confined beam effect occurs when the Poynting vector of the sum of E_h and E_t is nearly parallel to the crystal surface. In these works, the confined beam effect from a Ge crystal was studied using X-rays with energy near the K absorption edge of Ge. In the present case, the peak height at $y = H$ is smaller than that observed from Ge. This is because the imaginary part of the anomalous scattering factor is small for Si and the effect of anomalous transmission (Borrmann effect) is small.

5.3. Interference of two beams between BB^2 and BB^4 diffractions

In Fig. 3(*a*), a broad peak denoted as $P_h^{(3)}$ appears. This should be caused by the interference between the beams in BB^2 mode and in BB^4 mode, since the distance between $P_h^{(1)}$ and $P_h^{(3)}$ (A_3) is twice that between A_1 and A_2. If the interference intensity is calculated assuming these two beams are

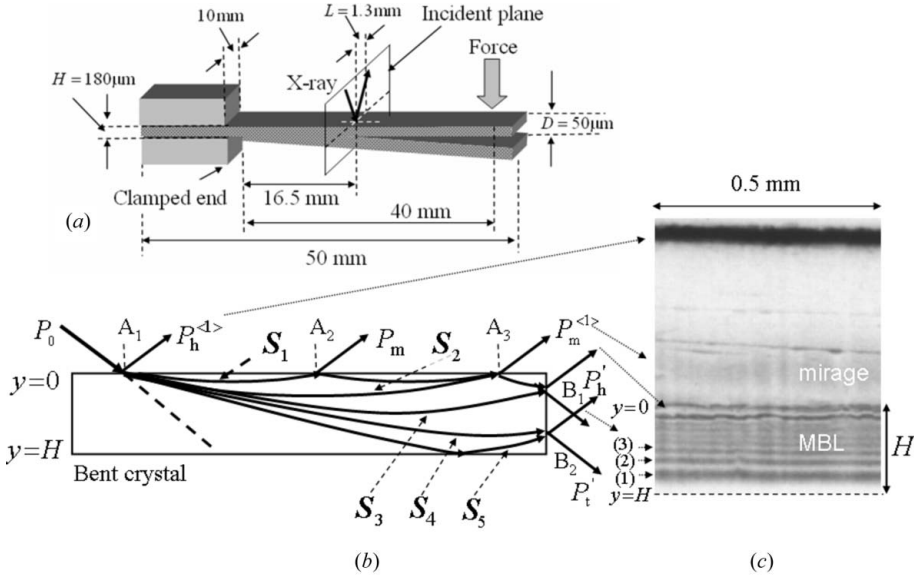

Figure 10
(*a*) The sample and the bending jig geometry. The sample is 50 mm long, 10 mm wide and 180 μm thick. The crystal is bent using a cantilever. Force is applied at the point 40 mm from the clamped end by moving the cantilever. The displacement is 50 μm. X-rays are incident at 16.5 mm from the clamped end and along the direction normal to the bending direction. The distance L is 1300 μm. (*b*) The beam geometry in a bent crystal. (*c*) Photograph of $P_h^{(1)}$, $P_m^{(1)}$ and P'_h.

coherent, two interference fringes should appear. But the difference in path length between the beam in BB^2 mode and that in BB^4 mode is approximately 50 μm, which is about three times larger than the coherent length (16 μm) in the present experiment. Since the beams in BB^2 mode and in BB^4 mode are incoherent with each other, no interference fringes appear and a broad peak $P_h^{(3)}$ results.

5.4. Bent crystal

A photograph taken from a bent crystal in the diffracted-beam direction is shown in Fig. 10(*c*). The sample size and the bending jig geometry are shown in Fig. 10(*a*). When the force is applied, the point of action is 40 mm from the clamped end and the displacement D is 50 μm. The corresponding beam geometry is shown in Fig. 10(*b*). The photograph shows the diffracted intensity $P_h^{(1)}$, mirage fringes $P_m^{(1)}$ and the diffraction from the lateral surface P_h'. The mirage fringes have been studied by Fukamachi *et al.* (2010). The fringes $P_m^{(1)}$ are observed in the beam coming out of the crystal at A_3. They are caused by interference between two mirage diffraction beams S_1 and S_2, as the paths of these beams in a bent crystal become hyperbolic forms (Gronkowski & Malgrange, 1984; Authier, 2001) as shown in Fig. 10(*b*), and come to the same point A_3. In Fig. 10(*c*), the peak (1) in the MBL interference fringes of P_h' appears at a position closer to the point $y = 0$ than expected for a flat crystal. This peak displacement can explain why the observed peak (1) in Figs. 3(*e*) and 3(*f*) appears closer to $y = 0$ as compared with the calculated peak in Figs. 9(*e*) and 9(*f*). It seems that the Si slice of crystal used in the measurement of MBL fringes in Figs. 3–6 may be distorted by gravity even when no force is explicitly applied to the slice.

6. Conclusions

The characteristics of the interference fringes in MBL modes from the surface and those from the lateral surface of an Si plane-parallel crystal have been analysed using coherence between the beams in MBL modes. When L/H is less than 15, the measured fringes are well reproduced by taking account of the interference between the two beams in BL and BBL modes. The small period of oscillations is additionally observed when L/H is larger than 15, which is reproduced by adding the beam in the higher-order MBL mode. The peak that appeared in the diffraction from the lateral surface shows some displacement closer to the surface side, which is explained by taking account of bending of the sample slice.

When L/H is larger than 15, a broad peak $P_h^{(3)}$ appears without any oscillatory part. As the difference in path length between two beams responsible for the interference is larger than the coherent length, no interference fringes occur. In addition, disappearance of the interference fringes for small values of y is also explained by considering the coherent length of the beams. The argument based on visibility of the interference fringes works quite well.

The number of interference fringes increases when the distance L decreases or the thickness H increases. The increase in number is useful for applications such as X-ray interferometry, as the interference fringes in MBL modes can be applied to interferometry using a bent crystal as well as using a flat crystal.

The authors would like to thank Professor Masayasu Tokonami of Saitama Institute of Technology and Dr Jun-ichi Yoshimura of KEK-PF for valuable discussions. This work was carried out under the approval of the Program Advisory Committee of PF (proposal No. 2008 G545). This work was partly supported by the 'Open Research Center' Project for Private Universities: 2007–2010 matching fund subsidy from MEXT (Ministry of Education, Culture, Sports, Science and Technology).

References

Authier, A. (2001). *Dynamical Theory of X-ray Diffraction.* Oxford University Press.
Fukamachi, T., Negishi, R., Yoshizawa, M. & Kawamura, T. (2005). *Jpn. J. Appl. Phys.* **44**, L787–L789.
Fukamachi, T., Negishi, R., Yoshizawa, M. & Kawamura, T. (2006). *Jpn. J. Appl. Phys.* **45**, 2830–2832.
Fukamachi, T., Negishi, R., Yoshizawa, M., Sakamaki, T. & Kawamura, T. (2004). *Jpn. J. Appl. Phys.* **43**, L865–L867.
Fukamachi, T., Tohyama, M., Hirano, K., Yoshizawa, M., Negishi, R., Ju, D., Hirano, K. & Kawamura, T. (2010). *Acta Cryst.* A**66**, 421–426.
Gronkowski, J. & Malgrange, C. (1984). *Acta Cryst.* A**40**, 507–514.
Hirano, K., Fukamachi, T., Yoshizawa, M., Negishi, R., Hirano, K. & Kawamura, T. (2009*a*). *Acta Cryst.* A**65**, 253–258.
Hirano, K., Fukamachi, T., Yoshizawa, M., Negishi, R., Hirano, K. & Kawamura, T. (2009*b*). *Phys. Status Solidi A*, **206**, 1855–1859.
Hirano, K., Fukamachi, T., Yoshizawa, M., Negishi, R., Hirano, K., Xu, Z. & Kawamura, T. (2008). *J. Phys. Soc. Jpn*, **77**, 103707.
Saka, T. & Kato, N. (1986). *Acta Cryst.* A**42**, 469–478.
Yoshizawa, M., Fukamachi, T., Hirano, K., Oba, T., Negishi, R., Hirano, K. & Kawamura, T. (2008). *Acta Cryst.* A**64**, 515–518.